Separation Science and Technology
Publication details, including instructions for authors and subscription information:
http://www.informaworld.com/smpp/title~content=t713708471

Vapor Permeation of Toluene, m-Xylene, and Methanol Vapors on Poly(Dimethylsiloxane) Membranes

Shingjiang Jessie Lue[a]; Wen Wei Chen[a]; Shao Fan Wang[a]
[a] Department of Chemical and Materials Engineering, Chang Gung University, Kwei-Shan, Taoyuan, Taiwan

To cite this Article Lue, Shingjiang Jessie , Chen, Wen Wei and Wang, Shao Fan(2009) 'Vapor Permeation of Toluene, m-Xylene, and Methanol Vapors on Poly(Dimethylsiloxane) Membranes', Separation Science and Technology, 44: 14, 3412 — 3434
To link to this Article: DOI: 10.1080/01496390903212615
URL: http://dx.doi.org/10.1080/01496390903212615

Separation Science and Technology, 44: 3412–3434, 2009

ISSN: 0149-6395 print/1520-5754 online
DOI: 10.1080/01496390903212615

Taylor & Francis
Taylor & Francis Group

Vapor Permeation of Toluene, m-Xylene, and Methanol Vapors on Poly(Dimethylsiloxane) Membranes

Shingjiang Jessie Lue, Wen Wei Chen, and Shao Fan Wang
Department of Chemical and Materials Engineering, Chang Gung University, Kwei-Shan, Taoyuan, Taiwan

Abstract: This study examined the simultaneous removal and recovery of volatile organic compounds (VOCs) from nitrogen streams using the vapor permeation (VP) technique. A poly(dimethylsiloxane) (PDMS) membrane was employed to separate toluene, m-xylene, and methanol from nitrogen gas. The effects of operating conditions (including PDMS cross-linker content, membrane thickness, feed flow rate, downstream pressure, and VOC feed concentration) on VOC removal were studied. The sorption isotherms and diffusion coefficients of the vapors in the PDMS were established using the gravimetric method. The Flory-Huggins equation was used to fit the vapor sorption isotherms in PDMS. The diffusivity dependence on vapor concentration were fitted using Long's model. The concentration distribution of the vapor in each layer was determined using a stack of membranes consisting of four layers. The measured permeant concentration distribution agreed excellently with the concentration profile calculation. The solution-diffusion model based on the first Fick's law can describe the mass-transfer mechanism of the vapors in a VP process.

Keywords: Concentration profile, diffusivity, poly(dimethylsiloxane) (PDMS), sorption, vapor permeation

Received 20 October 2008; accepted 25 June 2009.

Address correspondence to Shingjiang Jessie Lue, Department of Chemical and Materials Engineering, Kwei-Shan, Taoyuan County, 333 Taiwan. Tel.: +886-3-2118800 Ext. 5489; Fax: +886-3-2118700. E-mail: jessie@mail.cgu.edu.tw

INTRODUCTION

Volatile organic compound (VOC) emissions from many industrial processes (such as petroleum refining, printing, metal cleaning, painting, gluing, and coating) represent imperative environmental pollution and an economic loss problem. Although several procedures have been proposed for treating such organic vapors, these methods show some drawbacks in the prospective of efficiency and cost. Some treatments require regeneration and hence, encounter the disadvantage of changing the disposal problem into wastewater or dumping ground issue (1). According to Baker et al., solvents such as toluene, xylene, perchloroethylene, trichloroethane, ethyl alcohol, methyl alcohol, and acetone, are the major sources of solvent emissions (2).

The membrane-based vapor permeation (VP) technology has gained much attention recently because it can simultaneously remove organic vapors and recover solvents for reuse. This method involves the transfer of vapors from a gaseous mixture through a membrane into a low-pressure permeate side. The membrane material exhibits a selectivity that allows the passage of certain permeants while retaining others. For example, poly(dimethylsiloxane) (PDMS) has a higher affinity toward organic vapors than nitrogen and oxygen (2). Feeding a vapor-containing gas stream into a VP module is usually separated into two effluents: a VOC-lean gas stream and a VOC-enriched vapor phase. The latter may be condensed into liquids for reuse. Much research (1,3,4) has demonstrated that the VP process is economically feasible.

It is well accepted that the solution-diffusion model accounts for the mass-transfer mechanism in a VP process. The driving force is the permeant concentration gradient across the membrane. The sorbed vapor concentration is related to the vapor activity outside of the membrane and such relationship can be estimated from the sorption isotherm. The vapor transport takes place in three steps:

1. sorption of permeant(s) at the upstream membrane surface,
2. diffusion of the sorbed constituents through the membrane matrix, and
3. desorption from the membrane into the vapor phase at the permeate side (5).

The differentiation in solubility and/or diffusivity of the penetrants in the membrane governs the separation efficiency.

Some research has focused on organic vapor flux (or permeability) through polymers (1,2,4) in a VP process. The process design on vapor

permeability and selectivity were reported (6–10). Baertsch et al. (11) studied the VP permeability through silicalite-zeolite membranes fed with multi-component VOC streams. Lue et al. (12) reported the flux modeling of the multi-component mixtures in PDMS membrane.

This study investigated the effects of operating conditions (PDMS cross-linker content, membrane thickness, feed flow rate, downstream pressure, and VOC feed concentration) on VP performance using the PDMS membranes. The sorption, diffusion, and vapor permeation of the vapors (including methanol, toluene, and m-xylene) in PDMS during the VP process is elucidated. The permeant concentration profile inside the membrane is determined using Fick's first law and Long's model.

EXPERIMENTAL

Membrane Preparation

The PDMS membranes were prepared from two-component ingredients (KE-1310, both from Shin-Etsu Polymer Co., Ltd., Tokyo, Japan) by mixing ten parts of elastomer base with one part of the cross-linker in toluene (13). The amount of toluene was 1.5 times than that of the base. The solution was degassed in an ultrasonic bath at $10 \pm 1°C$ for 3 hours and the homogeneous solution was poured onto a plate. An adjustable film applicator (AP-M04, Gardner Co. Inc., Pompano Beach, Florida, USA) was placed at one edge of the solution and drawn slowly toward the other end to get a uniform polymer solution thickness. After curing at 80°C for 6 hours, the film became clear and transparent. The membrane sheet was peeled off and stored in a desiccator until use. A digital thickness gauge (model 345, Elcometer Instrument Ltd., Edge Lane, England) was used to measure the membrane thickness at 10 locations and the average thickness was recorded. The resulting dry membrane thickness was 60–65% of the clearance setting for the film applicator. The membrane density was about $1.091\ g/cm^3$. The mechanical properties (breaking strength, tensile strength, and elongation at break) were measured using a dynamic testing machine (Sintech 5/G, MTS Systems Co., Ltd., Eden Prairie, Minnesota, USA). The specimens were cut into strips of $5\,mm \times 30\,mm$. The samples were pulled at a rate of 10 mm/min according to the standard procedure (14). The coefficients of variation (defined as standard deviation divided by average) of these three quantities ranged from 3.1% to 6.1% from duplicate measurements.

VP Experiments

The VP apparatus set-up and the stainless steel membrane module were described in the previous paper (12). Organic vapors were generated from a bubbler placed into a thermostated bath. The vapors were diluted with nitrogen gas and thoroughly mixed prior to feeding into the membrane module. Gas flow meters (Restek Corp., Bellefonte, Pennsylvania, USA) and mass flow controllers (model 5850E, Brooks Inst., Hatfield, Pennsylvania, USA) were set so that a desired activity level could be achieved by adjusting suitable flow rates. The outlet of the permeate side was connected to an oil rotary vacuum pump (GVD-050A Ulvac, Shinku Kiko Co., Tokyo, Japan). A pirani vacuum gauge and controller (GP-ISRY, Ulvac, Shinku Kiko Co., Tokyo, Japan) were installed to maintain the pressure at 200 Pa. Two three-way valves were installed to allow the feed stream or the retentate stream to pass through a sampling valve connected to an on-line gas chromatograph (model 4890, Hewlett-Packard Co., Palo Alto, California, USA) for the VOC concentration measurement (12). Another flow meter was installed ahead of the gas chromatograph to determine the flow rates for the feed (Q_F) and the retentate (Q_R) streams. The vapor permeation flux was determined from the feed and retentate flow rates, and their vapor concentrations (N_F and N_R, respectively). Eqs. (1) and (2) show the mass balance for the total and vapor components:

$$Q_F = Q_R + Q_P \tag{1}$$

$$Q_F N_F = Q_R N_R + Q_P N_P \tag{2}$$

where Q and N represent flow rate and vapor concentration, subscripts F, R, and P for feed, retentate, and permeate, respectively. The permeate flow rate (Q_P) and its composition (N_P) were solved after Q_F, Q_R, N_F, and N_R were measured during the VP experiment.

The vapor permeation flux (J), the separation factor (α), and the removal efficiency (η) were used to characterize the VP performance:

$$J = Q_P N_P / A \tag{3}$$

$$\alpha = \frac{N_P/(\Lambda_T - N_P)}{N_F/(\Lambda_T - N_F)} \tag{4}$$

$$\eta = \left(1 - \frac{Q_R N_R}{Q_F N_F}\right) \times 100\% \tag{5}$$

where A is the effective membrane area, Λ_T the total number of gaseous moles per unit volume at a specified temperature, and pressure in a gas stream. The latter equals 40.82 mol/m^3 at 25°C and 1 atm in this study.

The apparent permeability (Π) was calculated by normalizing the flux with the membrane thickness (δ) and the partial pressure difference (ΔP):

$$\Pi = \frac{J\delta}{\Delta P} \tag{6}$$

The unit of Π is $\text{mol} \cdot \text{m}/\text{m}^2 \cdot \text{s} \cdot \text{Pa}$, and can be converted into Barrer (which is a more common unit in the gas separation area) by multiplying 2.99×10^{15}.

The operating conditions were as follows unless otherwise stated: effective membrane area of 18.1 cm^2, the feed pressure of 101.3 kPa, the downstream pressure of 200 Pa, the temperature of 25°C, the feed flow rate of 2.37×10^{-6} m^3/s (140 cm^3/min), membrane thickness of 180 μm, and a weight ratio of polymer base to cross-linker for PDMS of 10 to 1.

Sorption Experiments

The vapor sorption experiments were carried out at a temperature of 25°C using a sorption apparatus equipped with a Sartorius electronic microbalance (model BP211D, Sartorius AG, Goettingen, Germany). Membrane samples weighing 0.3–1.0 g were suspended in a chamber filled with organic vapor at various activity levels. The mass uptake of these membranes was measured at specified time intervals until the equilibrium was reached.

The equilibrium vapor uptake (M_∞, in g/g membrane) as a function of vapor activity was used to establish the sorption isotherm. The detailed procedures are described in our recent publications (15). Flory-Huggins thermodynamics (16) was used to describe the equilibrium solvent uptake at different vapor activity as follows:

$$\ln a = \ln \frac{P}{P^o} = \ln \phi_1 + \left(1 - \frac{V_1}{V_M}\right)(1 - \phi_1) + \chi_{1M}(1 - \phi_1)^2 \tag{7}$$

where P is the partial vapor pressure, P^o is the saturated vapor pressure at 25°C, ϕ_1 is the volume fraction of permeate in polymer, χ_{1M} is the Flory-Huggins interaction parameter between penetrant and membrane, and V_1 and V_M are the molar volumes of the penetrant and the membrane, respectively. The saturated vapor pressure was calculated using

the Antoine equation as described elsewhere (12). After the vapor uptake M_t (g vapor/g membrane) was determined, the vapor volume fraction ϕ_1 was calculated from the densities of the solvent and the membrane (12). The interaction parameter could be calculated using the least squares method using Eq. (7).

Measurement of Diffusion Coefficients

The gravimetric method was used to measure the vapor diffusion coefficients as described in the sorption experiment section and in our previous paper (17). The vapor mass uptakes at various time intervals (M_t, in g/g membrane) were recorded. The kinetic sorption data prior to equilibrium was used to calculate the corresponding diffusion coefficient of that particular vapor in the PDMS film. When the membrane was surrounded in a saturated vapor, the sorption behaviors resembled the Fickian kinetic and the diffusion coefficient was determined using the Balik method (18):

$$\frac{M_t}{M_\infty} = \varphi(x)\left(\frac{4}{\delta}\sqrt{\frac{Dt}{\pi}}\right) + [1 - \varphi(x)]\left[1 - \frac{8}{\pi^2}\exp\left(\frac{-\pi^2 Dt}{\delta^2}\right)\right] \tag{8}$$

where M_t and M_∞ are solvent uptake (g/g dry membrane) at time t and at equilibrium, respectively; t is the elapsed time (s); D is the diffusion coefficient (m^2/s) and δ the membrane thickness (m), φ (x) is a Fermi function shown in Balik (18). This procedure was performed when a container half full of the vapor-liquid solvent was raised toward a dry membrane suspended underneath a micro-balance (17).

In cases where the membrane was immersed in an unsaturated vapor which was produced by mixing nitrogen into a vapor stream as described in the sorption experiment section, the sorption kinetic was a sigmoid curve (17). A nonlinear regression model (17,19,20) was used to fit the diffusion coefficient:

$$\begin{aligned}\frac{M_t}{M_\infty} = {} & 1 - \exp(-\beta t)\left(\frac{4D}{\beta\delta^2}\right)^{1/2}\tan\left(\frac{\beta\delta^2}{4D}\right)^{1/2} \\ & - \frac{8}{\pi^2}\sum_{n=0}^{\infty}\frac{\exp[-(2n+1)^2\pi^2 Dt/\delta^2]}{(2n+1)^2[1 - (2n+1)^2 D\pi^2/(\beta\delta^2)]}\end{aligned} \tag{9}$$

where β is a parameter used to characterize the deviation in the non-perfect step change at the initial vapor sorption period (19) and can be determined experimentally (20).

Determination of Concentration Profiles of Vapors inside PDMS

Four layers of the PDMS membrane were stacked together and installed in the membrane module for vapor permeation. The vapor permeation flux through the stack was calculated using the procedure in the VP experiment aforementioned. After the VP experiment was completed, the membrane stack was removed and the solvent concentration in each layer was determined using a purge-and-trap unit (model 4560, O.I. Analytical Corp., College Station, Texas, USA) and a gas chromatograph (15).

Fick's first law (Eq. (10)) was used to derive the concentration profile inside the PDMS.

$$J = -D\frac{dC}{dx} \tag{10}$$

where J is the vapor flux, D is the diffusion coefficient, C is the vapor concentration in the membrane, and x is the distance away from the upstream membrane surface along the trans-membrane direction. The diffusivity dependency on the solvent concentration was estimated using Long's model:

$$D = D_0 \exp(\gamma C) \tag{11}$$

where D_0 is the infinite dilution diffusion coefficient and γ is the plasticization coefficient.

Substituting Eq. (11) into Eq. (10) and integrate the equation, one can obtain:

$$\exp(\gamma C) = \exp(\gamma C_F) - \frac{Jx\gamma}{D_0} \tag{12}$$

where C_F is the solvent concentration at the upstream surface and can be estimated from the sorption isotherm under a predetermined vapor activity with a known χ_{1M} value, as shown in Eq. (7). The solvent concentration at any location (distance of x) in the membrane (C) can be determined from Eq. (12) with known values of J, γ, $D_{0,}$ and C_F.

RESULTS AND DISCUSSION

Effect of Cross-Linker Content of PDMS on Permeability

In a preliminary study, various weight ratios (10:1∼10:5) of the base to the cross-linker were tried out for making PDMS and the effects on

Table 1. VP properties of PDMS with various base/cross-linker weight ratios[a]

Weight ratio of base:cross-linker	Flux (10^{-3} mol/m^2 s)	Apparent permeability (10^{-11} mol m/m^2 s Pa)[b]	Separation factor
10:1	2.11	10.0 (2.99×10^5)	159
10:2	2.24	10.6 (3.17×10^5)	169
10:4	2.30	10.9 (3.25×10^5)	174
10:5	2.21	9.38 (2.80×10^5)	158

[a]Effect membrane area: 18.1 cm^2, temperature: 25°C, downstream pressure: 200 Pa, feed flow rate: 140 cm^3/min; membrane thickness: 180 μm; feed mixture: toluene/nitrogen (activity 0.94–1.0).

[b]Values in the parentheses following the data are in Barrer unit.

the vapor permeation properties were studied. The flux, the apparent permeability, and the separation factor in the 10:4 membrane was slightly higher than the other tested samples (Table 1). The vapor removal efficiency was 64–73%. This slight deviation was speculated due to the increase of the fractional free volume resulted from the incorporation of the cross-linker in the sample preparation step. As more cross-linker was added into the polymer solution, the higher content of the end groups tend to polymerize and inhibit the vapor transport. Although the PDMS with a weight ratio of 10:4 gave the highest permeability and separation factor, the difference between the results from this recipe and 10:1 sample was probably within the experimental error as mentioned in the next paragraph. Since the base-to-cross-linker ratio of 10:1 was recommended by the manufacturer, this recipe was used throughout the experimental runs.

The 10:1 base-to-cross-linker ratio was used to cast PDMS films about 180 μm in thickness. In replicate tests, the membrane thickness was 186 ± 4 μm (mean± standard deviation) and the measured toluene permeability was $0.84–1.09 \times 10^{-10}$ mol·m/m$^2 \cdot$ s $\cdot$ Pa (2.51–3. 26×10^5 Barrer). These results were one order of magnitude higher than what (25000 Barrer) was reported by Paul et al. (4) but close to Blume et al.'s data (2). The toluene/nitrogen separation factor was 146–172, which was comparable to literature value of 183 (6).

Effect of Membrane Thickness on Mechanical Properties

The 10:1 base-to-crosslinker ratio was used to cast PDMS films of various thicknesses. The effect of the membrane thickness on the mechanical properties was investigated. The tensile strength and the elongation at

Table 2. The mechanical properties of PDMS with various thicknesses[a]

Thickness (μm)	33	85	186	265
Tensile strength (Mpa)	1.823	1.911	1.970	2.117
Elongation (%)	94.80	120.2	198.9	250.7

[a]Weight ratio of base/cross-linker was 10:1.

break were enhanced with the thicker membrane (Table 2). The toluene/nitrogen separation factors of 33- and 85-μm films were lower than those of 186- and 265-μm films. The thinner films may have defects or pin-holes and render leakage for nitrogen, resulting in low separation efficiency. In the subsequent runs, the membrane thickness of ~180 μm was used to ensure the representative and the reliable data obtained.

Effect of Feed Flow Rate

Increasing the feed flow rate favored both the permeability and the separation factor employing this membrane module design (12) (Fig. 1). Some studies indicated that high flow rates result in high permeability and separation factor but the benefits level off after reaching a certain

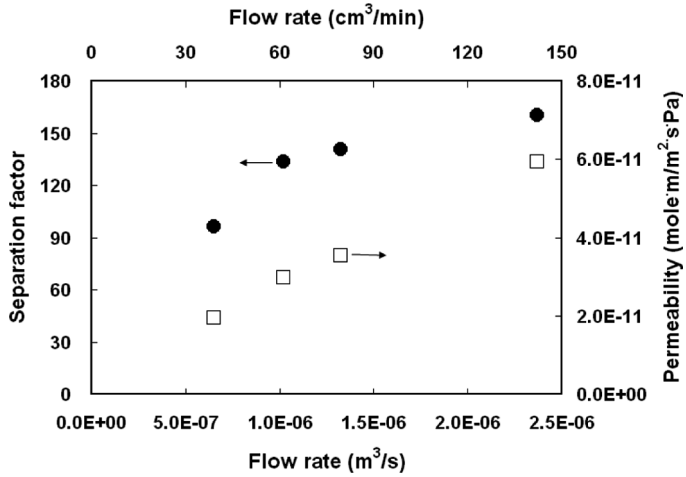

Figure 1. Feed flow rate effect on toluene separation factor and apparent permeability (downstream pressure: 200 Pa, membrane thickness: 180 μm, and temperature: 25°C).

value (9). This increase may be explained by the decreased vapor mass-transfer resistance associated with a high flow rate in the boundary layer of the feed regime (22). A high flow rate increases the Reynolds number of the feed stream. The mass transfer coefficient then increases with the Reynolds number to the order of 0.33 for laminar flow (23). The higher mass transfer coefficient reduces the boundary layer in the feed stream and causes less concentration polarization in the boundary regime, as shown in Fig. 2a. The vapor solubility therefore was enhanced and a higher vapor flux was resulted. A similar effect was reported in the pervaporation of benzene from aqueous solution using the PDMS/non-woven composite (24). However, the benefit of increasing the flow rate will not continue infinitely. As the flow rate increases to a certain level, the penetrant sorption into the membrane approaches the equilibrium sorption level and is no longer a limiting step and the situation becomes a diffusion-limited process as described as follows.

The increases in the Reynolds number also enhance the vapor selectivity. Within the boundary layer, the concentration profile changes because the faster permeating component is depleted (as shown in Fig. 2b) and the slower species is enriched. Therefore, the effective driving force

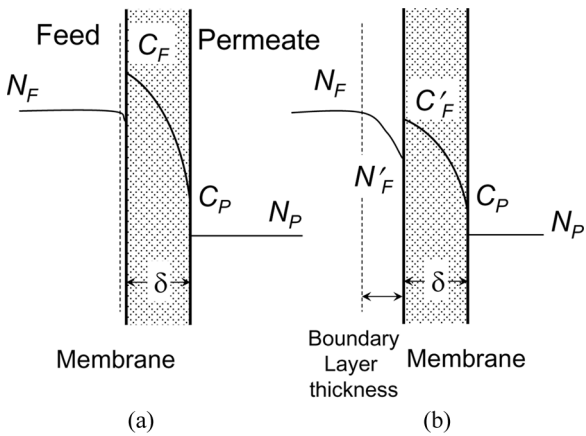

Figure 2. Illustration showing the cross-sectional view of vapor concentration polarization in a VP process: (a) negligible boundary layer thickness at high flow rate and; (b) significant boundary layer thickness. The vapor concentration at the feed-membrane interface (C_F or C'_F) is in equilibrium with the vapor composition in the feed (N_F or N'_F), and the vapor concentration at the permeate-membrane interface (C_P) is in equilibrium with the vapor composition in the permeate (N_P). The concentration gradient across the membrane thickness (δ) is the driving force for vapor transport.

for the faster component (vapor in this study) is reduced and the slower nitrogen gas has higher driving force due to the accumulated concentration near the feed-membrane interface. The separation factor is consequently lowered at a slower feed rate, as shown in Fig. 1. Conversely, increasing the flow rate helped to reduce the boundary layer thickness and lessen the concentration polarization (as shown in Fig. 2a). The separation factor was improved. For example, Alpers et al. (23) reported that both the n-butane mass transfer coefficient and n-butane/nitrogen selectivity increase with increasing Reynolds number in the vapor permeation process.

Effect of Downstream Pressure

A solution-diffusion model is often used to describe the mass transfer mechanism during the VP processes. Most mass-transfer models utilizing a dense membrane are based on the assumptions that the diffusion is a rate-limiting step and that the penetrant sorption (or solution) in the membrane phase is in equilibrium with the vapor phase in the feed, as shown in the negligible boundary layer thickness in Fig. 2a. A low downstream pressure (i.e., high vacuum) facilitates the mass transfer by lowering the equilibrium vapor concentration downstream. The downstream pressure effects on the vapor permeability and separation factor are shown in Fig. 3. Decreasing the downstream pressure would enlarge the driving force (concentration gradient) and therefore increase the permeability and flux, as observed in a pervaporation process (24,25). Shelden and

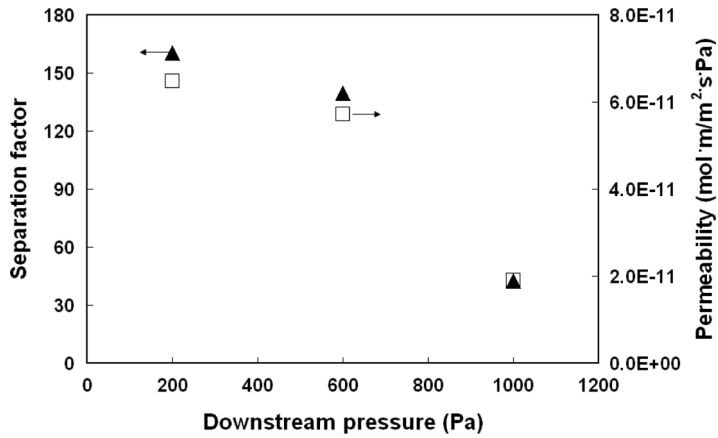

Figure 3. Downstream pressure effect on toluene separation factor and apparent permeability (flow rate: $2.37 \times 10^{-6}\,m^3/s$, membrane thickness: 180 μm, and temperature: 25°C).

Thompson (26) and Greenlaw et al. (27) proposed that the selectivity depends upon the membrane-permeant characteristics. Our results indicate that the separation factor was higher at a lower downstream pressure.

Effect of Vapor Activity on Vapor Flux

The flux dependency on the vapor activity was determined using VOC/nitrogen mixture. Figure 4 demonstrates the vapor flux as a function of various vapor activities in the feed stream. Increasing the vapor activity in the feed resulted in a greater driving force, which would increase the sorption concentration (C_F in Fig. 2) and the vapor flux (3,9,12), as shown in Fig. 4. The measured apparent permeability of m-xylene was $5.4–7.8 \times 10^{-11}$ mol · m/m^2 · s · Pa (or $1.6–2.3 \times 10^5$ Barrer, as shown in Fig. 5), which was not significantly different from that of toluene ($4.5–6.8 \times 10^{-11}$ mol · m/m^2·s · Pa or $1.3–2.0 \times 10^5$ Barrer). The permeability of methanol was the lowest among the tested vapors ($1.1–2.0 \times 10^{-11}$ mol · m/m^2 · s · Pa or $3.2–5.9 \times 10^4$ Barrer) (Fig. 5).

The vapor removal efficiency was determined according Eq. (5) and the results are shown in Fig. 6. Toluene and m-xylene vapors were removed by 50–78%, while methanol was only reduced by 12–24%. The ease of vapor abatement was in the similar trend as the apparent permeability data of the VOCs.

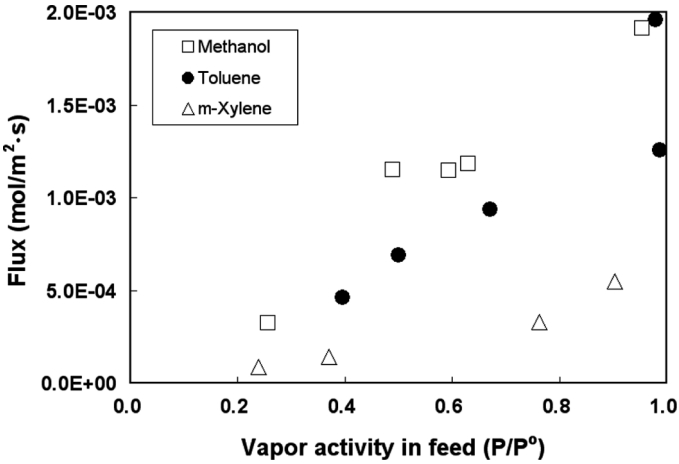

Figure 4. Vapor permeation flux from VOC/nitrogen mixture at various activity levels (flow rate: 2.37×10^{-6} m^3/s, membrane thickness: 180 μm, temperature: 25°C, and downstream pressure: 200 Pa).

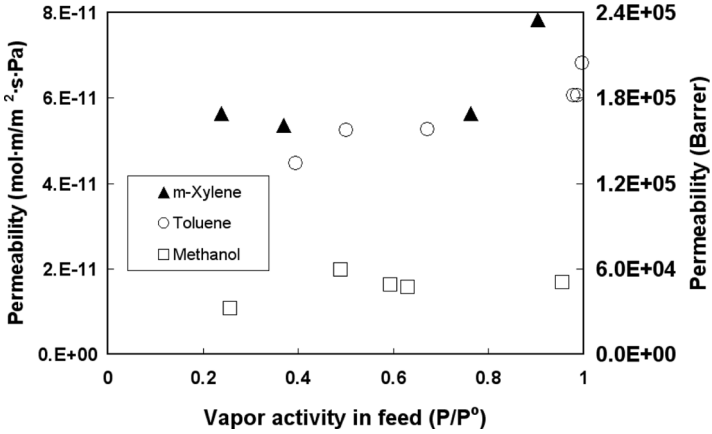

Figure 5. Vapor apparent permeability from VOC/nitrogen mixtures at various activity levels (flow rate: $2.37 \times 10^{-6}\,m^3/s$, membrane thickness: 180 μm, temperature: 25°C, and downstream pressure: 200 Pa).

Vapor Sorption Isotherms

To elucidate the sorption behavior of VOCs on a PDMS membrane, the equilibrium vapor uptake was measured at different activities. The data indicates that the Flory-Huggins model adequately described the sorption

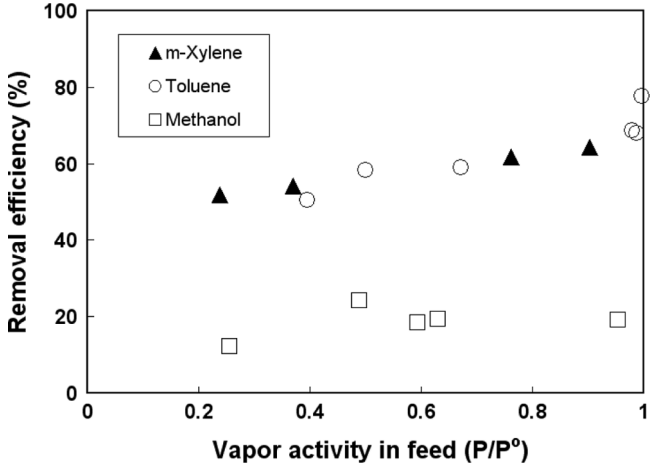

Figure 6. Vapor removal efficiency from VOC/nitrogen mixtures at various activity levels (flow rate: $2.37 \times 10^{-6}\,m^3/s$, membrane thickness: 180 μm, temperature: 25°C, and downstream pressure: 200 Pa).

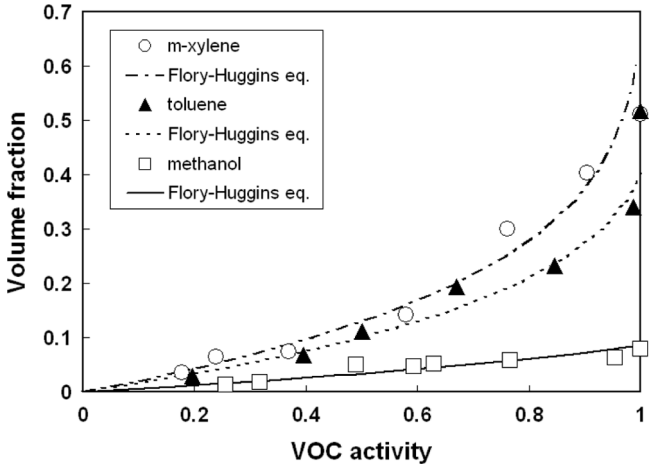

Figure 7. Sorption isotherms and the Flory-Huggins models at a temperature of 25°C.

prediction. Figure 7 shows the sorption data and the fitted curves based on the Flory-Huggins equations (Eq. (7)). The toluene and m-xylene exhibit higher solubility in PDMS (about 0.86 g/g, as indicated in Table 3). The methanol was only slightly soluble in PDMS with a sorption uptake of 0.06 g/g. These sorption uptakes can be explained in terms of chemical compatibility. The PDMS has a solubility parameter of 14.9–15.6 $J^{1/2}/cm^{3/2}$, which is closer to those of m-xylene (17.9–18 $J^{1/2}/cm^{3/2}$) and toluene (18.2–18.3 $J^{1/2}/cm^{3/2}$) (28). The methanol is more hydrophilic and has a solubility parameter of 29.2–29.7 $J^{1/2}/cm^{3/2}$. The methanol sorption uptake was smaller than the other two vapors due to the higher difference in the chemical compatibility with PDMS.

Table 3. Physico-chemical properties of vapors and PDMS

Component	Density (g/cm^3)	Molecular weight (g/mol)[a]	Solubility parameter ($J^{1/2}/cm^{3/2}$)[a]	Flory-Huggins interaction parameter, χ_{1M}	Sorption uptake in PDMS (g/g)
Methanol	0.792[a]	32.04[a]	29.2–29.7	1.852 ± 0.167	0.062 ± 0.006
Toluene	0.867[a]	92.13[a]	18.2–18.3	0.886 ± 0.114	0.858 ± 0.017
m-Xylene	0.864[a]	106.16[a]	17.9–18.0	0.650 ± 0.143	0.857 ± 0.053
PDMS	1.091	17300[b]	14.9–15.6	–[c]	–[c]

[a]Data from Van Krevelen (28).
[b]Mn = 17300, Mw/Mn = 2.47 (13).
[c]Not applicable.

The Flory-Huggins interaction parameters were 0.64, 0.89, and 1.85 for m-xylene, toluene, and methanol, respectively. The predicted volume fractions as a function of the vapor activity for each vapor were plotted and compared with the experimental data in Fig. 7. All these sorption isotherms exhibited a concave trend and the volume fraction increased at a higher rate at higher activity levels. It has been proposed that the Flory-Huggins interaction parameter is related to the difference in the solubility parameters of a permeant and membrane (28):

$$\chi_{1M} = 0.34 + \frac{V_1}{RT}(\Delta_M - \Delta_1)^2 \tag{13}$$

where R is the gas constant, T is the absolute temperature, V_1 is the molar volume of the permeant, Δ_1 and Δ_M are the solubility parameter for the permeant and the membrane, respectively. From Eq. (13) and the data in Table 3, one can estimate the χ_{1M} values of 0.70, 0.73, and 3.67 for m-xylene, toluene, and methanol, respectively. Our measured data were in accordance with the estimated ones and we obtained the lowest Flory-Huggins interaction parameter for m-xylene and PDMS due to the closer solubility parameters between these two.

Vapor Diffusion Coefficients

The transient sorption data were recorded from the micro-balance during the sorption measurement. Some typical results are shown in Fig. 8. These data sets were analyzed to extract the diffusion coefficients using the procedure described in our earlier paper (17,19). The diffusion coefficients were 2.51×10^{-11} $-4.89 \times 10^{-11}\,m^2/s$ for m-xylene, 2.24×10^{-11} $-5.77 \times 10^{-11}\,m^2/s$ for toluene, and 6.6×10^{-11} $-4.69 \times 10^{-10}\,m^2/s$ for methanol, as shown in Fig. 9. Each diffusion coefficient can be treated as the average value for a vapor with concentrations ranging from zero to the equilibrium uptake (M_∞, which can be predicted from the sorption isotherms at a given activity level from Fig. 7). Therefore the diffusion coefficient was associated with an average vapor concentration of $M_\infty/2$. By applying the Long's model (Eq. (10)) one can obtain the parameters D_0 and γ for each vapor, as shown in Fig. 10.

The fitted D_0 values represent the vapor diffusion coefficient at infinite dilution (i.e., zero concentration). The methanol molecule is the smallest in size among the tested vapor components and exhibited the largest D_0 value ($9.16 \times 10^{-10}\,m^2/s$). On the other hand, the largest m-xylene molecule showed the slowest intrinsic diffusivity with a D_0 of $3.09 \times 10^{-11}\,m^2/s$. The γ data describe the plasticization effect of the

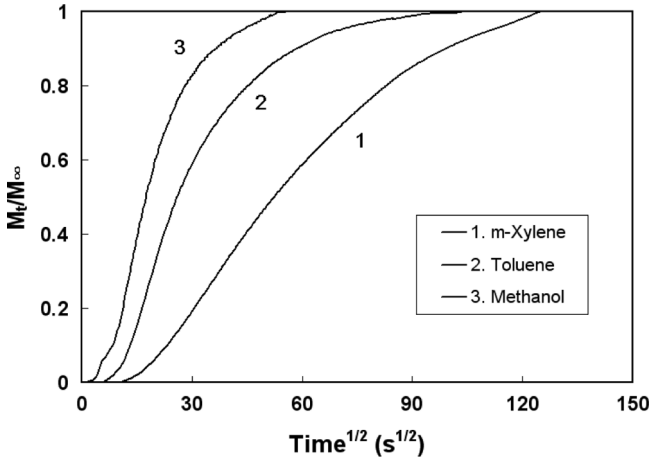

Figure 8. Typical transient sorption regimes for vapors in PDMS (operating condition for m-xylene: activity of 0.711 and membrane thickness of 287 μm; for toluene: activity of 0.40 and membrane thickness of 268 μm; for methanol: activity of 0.741 and membrane thickness of 180 μm).

sorbed vapor molecules on the future vapor diffusivity. Generally speaking, pre-sorbed vapor usually plasticizes the polymer matrix and makes it more flexible and readily available for permeant diffusion. This phenomenon was observed in the m-xylene and PDMS system: the

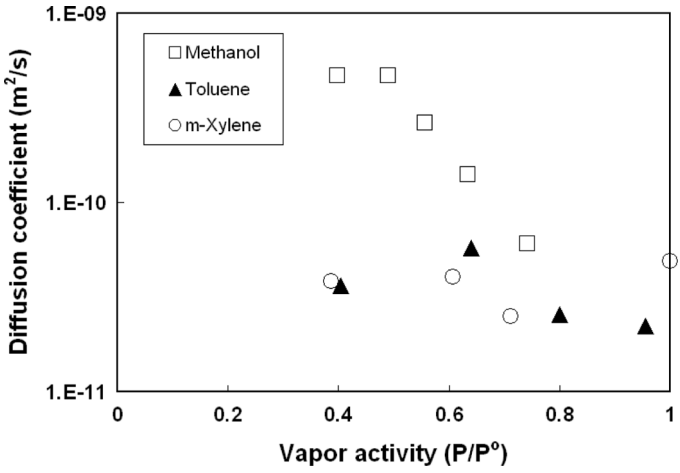

Figure 9. Vapor diffusion coefficients form VOC/nitrogen mixtures of various activity levels.

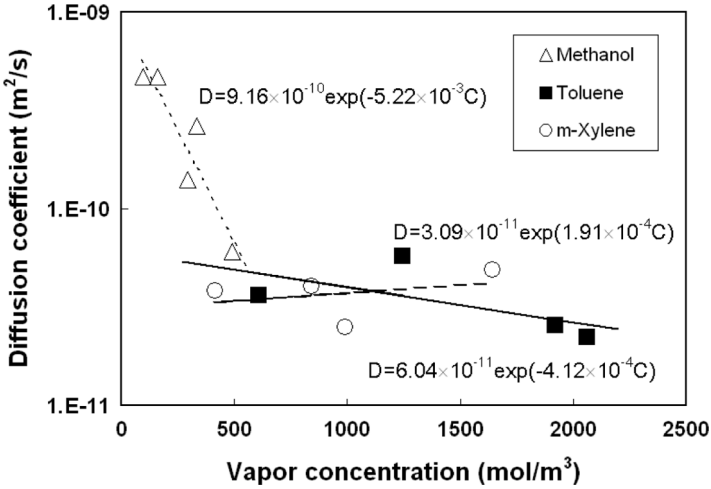

Figure 10. Vapor diffusion coefficients form VOC/nitrogen mixtures as a function of vapor concentration in membrane.

molecular diffusion coefficient was enhanced by increasing the vapor activity. A positive γ value, 1.91×10^{-4} m^3/mol, was obtained for m-xylene. For toluene and methanol the opposite trend was noted: the molecular diffusion coefficient was retarded at the high activity levels. This may be due to the reduction in the fractional free volume (12,29) with the pre-sorbed vapor occupancy. The toluene and methanol diffusion coefficients declined with sorption levels. Negative γ values of -4.12×10^{-4} m^3/mol and -5.22×10^{-3} were found for toluene and methanol, respectively.

Although methanol had the highest diffusion coefficient (Fig. 9), the low sorption uptake hindered its mass transfer, resulting in the lowest apparent permeability (Fig. 5). m-Xylene exhibited the most sorption uptake in PDMS (Fig. 7), demonstrated the highest permeability property (Fig. 5). The sorption behavior (related to the thermodynamic phenomenon) and the diffusion pattern (a dynamic term in nature) altogether govern the vapor permeation properties. The solution-diffusion model based on the first Fick's law (Eq. (10)) can describe the vapor flux in a VP process.

Vapor Concentration Profile within Membrane

The permeation flux of the vapor through the multiple-layer stack of PDMS membrane was summarized in Table 4. The vapor concentration in the membrane at the feed-membrane interface (i.e., C_F in Fig. 2) is estimated from the sorption isotherm in Fig. 7. The vapor concentration

Table 4. VP performance of vapor/nitrogen mixtures in multiple-layer stack of PDMS membrane[a]

Vapor	Total membrane thickness (μm)[b]	Vapor activity	Flux (10^{-4} mol/m$^2 \cdot$ s)	Apparent permeability (Barrer)
Methanol	510	0.758	2.22	26500
Toluene	515	0.956	6.65	242000
m-Xylene	529	0.735	1.86	362000

[a]Effective membrane area: 18.1 cm^2; temperature: 25°C, downstream pressure: 200 Pa. Feed flow rate: 121 cm^3/min for methanol and m-xylene, 124 cm^3/min for toluene.

[b]Individual layer thickness is 110–144 μm for methanol, 123–135 μm for toluene, 119–140 μm for m-xylene.

in various locations within the PDMS was calculated according to Eq. (12) after J, C_F, D_0, and γ were determined as described in the previous sections. The profiles along the trans-membrane direction are shown in the curves in Fig. 11. The bars represent the measured vapor concentrations for the four layers, arranged from the feed to the permeate interface, during the VP operation. The error bars represented the standard deviations resulting from the analytical methods. The concentration profile of each compound in the membrane is quite different from the others. The highest concentration occurred at the feed interface and depended on the vapor activity and the sorption behavior. A high vapor activity and a low Flory-Huggins parameter (χ_{iM}) tends to exhibit a high concentration at the feed interface (corresponding to $x = 0$), as shown for m-xylene and toluene in Figs. 11a and b. Methanol had low solubility in the membrane and the vapor concentration at the feed interface was smaller than the other vapors (Fig. 11c).

The curvatures in the permeant concentration profiles are different for various vapors. If the vapor diffusivity is independent on its sorption level (i.e., constant D value in Eq. (10)), the concentration profile will become a straight line because dC/dx will be a constant equaling J/D. This inference is based on the assumption that at a steady state the flux (J) through various slices within the membrane is the same and no accumulation occurs. For a positive γ value, D increases with sorption

Figure 11. (a) m-Xylene; (b) toluene, and; (c) methanol concentration profiles in PDMS along trans-membrane direction (location 0 indicating feed-membrane interface, temperature: 25°C, downstream pressure: 200 Pa, and effective membrane area: 15.9 cm^2) ((a) flow rate: 2.01×10^{-6} m^3/s, total membrane thickness: 529 μm; (b) flow rate: 2.07×10^{-6} m^3/s, total membrane thickness: 515 μm; (c), flow rate: 2.02×10^{-6} m^3/s, total membrane thickness: 510 μm).

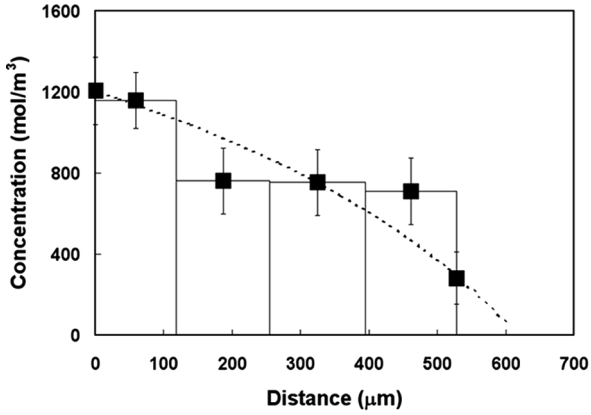

(a)

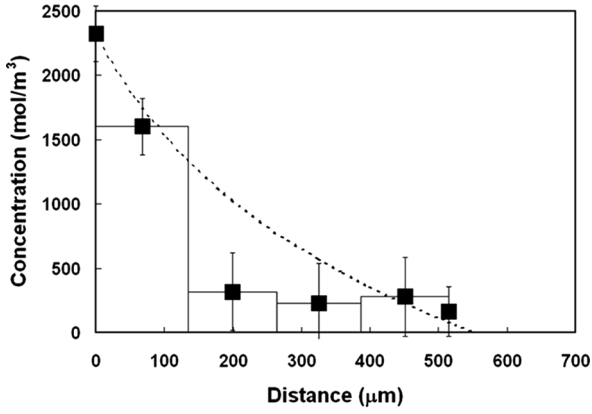

(b)

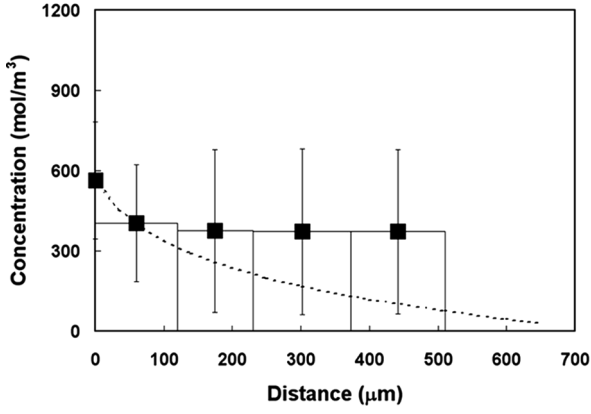

(c)

concentration (C) and the profile becomes convex in order to maintain a constant D(dC/dx) value. This value equals the vapor flux and should remain the same at a steady state condition. Under this circumstance, the slope at the concentration profile is low at the high concentration regime (at a location close to feed interface) because the D value therein is high. The profile in Fig. 11a demonstrates this example. Conversely, a concave profile is expected for a negative γ value. The concentration decrease is more pronounced near the feed interface in order to counterbalance the smaller diffusivity at this high sorption level. The toluene and methanol concentration profiles in Fig. 11b and c illustrate this pattern. The data in Fig. 11 clearly demonstrate that the experimental results coincide with the predicted curves. The plasticization coefficient (γ) in the Long's equation can serve as an indicator to describe the vapor concentration distribution and the profile curvature within the PDMS.

CONCLUSIONS

The operating condition effects (PDMS cross-linker content, feed flow rate, downstream pressure, and vapor feed concentration) on the VP permeability and separation efficiency were investigated. The vapor apparent permeability increased with the high flow rate, the low downstream pressure, and the increased feed concentration. The separation factor was higher using thicker membranes, a higher feed flow rate, and lower downstream pressure.

VOC sorption isotherms and diffusion coefficients in PDMS were established using the gravimetric method. The vapor uptake was in the decreasing order: m-xylene, toluene, and methanol. The Flory-Huggins model explained the sorption isotherm successfully and the interaction parameters between the VOCs and PDMS were determined. The diffusion coefficients of the VOCs were measured from the sorption kinetic data. Methanol showed the highest diffusion coefficient, followed by toluene, and m-xylene. Their diffusivity values are fitted using the Long's model as a function of the vapor concentration. The measured concentration profile agreed very well with the results derived from the Long's model, further confirming the adequacy of the mass transfer model.

ACKNOWLEDGEMENT

Thanks are due to National Science Council (NSC 92-2622-E-182-010-CC3) and Chang Gung University (BMRP326) for the financial support. Valuable discussion with the Referees is greatly acknowledged.

NOMENCLATURE

A	membrane area (m^2)
a	vapor activity (dimensionless)
C	vapor concentration in membrane (mol/m^3)
D	vapor diffusion coefficient (m^2/s)
D_0	diffusion coefficient at zero concentration (m^2/s)
J	vapor flux (mol/m^2s)
M	vapor uptake (kg/kg)
N	vapor concentration in gaseous stream (mol/m^3)
P	vapor pressure (Pa)
P^o	saturated vapor pressure (Pa)
ΔP	vapor partial pressure difference (Pa)
Q	gas flow rate (m^3/s)
t	time (s)
V	molar volume (m^3/mol)
x	distance from feed-membrane interface (m)

Subscript

1	vapor component
F	feed
M	membrane
P	permeate
R	retentate
T	total
t	time t
∞	at equilibrium

Greek Letters

α	separation factor (dimensionless)
β	parameter characterizing non-step change of vapor concentration during sorption experiment (1/s)
χ_{1M}	Flory-Huggins interaction parameter (dimensionless)
δ	membrane thickness (m)
Δ	solubility parameter ($J^{1/2}/cm^{3/2}$)
ϕ	volume fraction of solvent in membrane (dimensionless)
γ	plasticizing coefficient (m^3/mol)
η	vapor removal efficiency (dimensionless)
φ (x)	Fermi function shown in Balik (18) (dimensionless)
Λ	number of moles per unit volume in a gaseous stream (mol/m^3)
Π	apparent vapor permeability ($mol \cdot m/m^2 \cdot s \cdot Pa$ or Barrer)

REFERENCES

1. Kimmerle, K.; Bell, C.M.; Gudernatsch, W.; Chmiel, H. (1988) Solvent recovery from air. *J. Membrane Sci.*, *36*: 477–488.
2. Baker, R.W.; Yoshioka, N.; Mohr, J.M.; Khan, A.J. (1987) Separation of organic vapors from air. *J. Membrane Sci.*, *31* (2–3): 259–271.
3. Leemann, M.; Eigenberger, G.; Strathmann, H. (1996) Vapor permeation for the recovery of organic solvents from waste air streams: Separation capacities and process optimization. *J. Membrane Sci.*, *113* (2): 313–322.
4. Paul, H.; Philipsen, C.; Gerner, F.J.; Strathmann, H. (1988) Removal of organic vapors form air by selective membrane permeation. *J. Membrane Sci.*, *36*: 363–372.
5. Cen, Y.; Lichtenthaler, R.N. (1995) Vapor permeation. In: *Membrane Separations Technology; Principles and Applications*, Noble, R.D.; Stern, S.A. eds.; Elsevier Science: Amsterdam, 85–112.
6. Matsumoto, K.; Ishii, K.; Kuroda, T.; Inoue, K.; Iwama, A. (1991) Membrane process for organic vapor recovery form air. *Polym. J.*, *23* (5): 491–499.
7. Ohlrogge, K.; Brockmoller, J.; Wind, J.; Behling, R.D. (1993) Engineering aspects of the plant design to separate volatile hydrocarbons by vapor permeation. *Sep. Sci. Technol.*, *28* (1): 227–240.
8. Baker, R.W.; Wijmans, J.G.; Kaschemekat, J.H. (1998) The design of membrane vapor-gas separation systems. *J. Membrane Sci.*, *151* (1): 55–62.
9. Cha, J.S.; Malik, V.; Bhaumik, D.; Li, R.; Sirkar, K.K. (1997) Removal of VOCs from waste gas streams by permeation in a hollow fiber permeator. *J. Membrane Sci.*, *128* (2): 195–211.
10. Bhaumik, D.; Majumdar, S.; Sirkar, K.K. (2000) Pilot-plant and laboratory studies on vapor permeation removal of VOCs from waste gas using silicone-coated hollow fibers. *J. Membrane Sci.*, *167* (1): 107–122.
11. Baertsch, C.D.; Kunke, H.H.; Falconer, J.L.; Noble, R.D. (1996) Permeation of aromatic hydrocarbon vapors through silicalite-zeolite membranes. *J. Phys. Chem.*, *100*: 7676–7679.
12. Lue, S.J.; Chen, W.W.; Wu, S.Y.; Wang, L.D.; Kuo, C.H. (2008) Vapor permeation modeling of multi-component systems using a poly(dimethylsiloxane) membrane. *J. Membrane Sci.*, *311* (1–2): 380–389.
13. Lue, S.J.; Yang, S.W.; Chang, Y.S. (2006) Sorption of organic solvents in poly(dimethyl siloxane) membrane II. Effect of sorption on the polymer crystalline upon cooling. *J. Macromol. Sci., Part B Phys.*, *45* (3): 417–430.
14. ASTM (1994), *Annual Book of ASTM Standards*, Designation D 638–91: Standard test method for tensile properties of plastics; American Society for Testing and Materials: West Conshohocken, PA, USA.
15. Lue, S.J.; Wu, S.Y.; Wang, S.F.; Wang, L.D.; Tsai, C.L. (2008) Modeling multi-component vapor sorption in a poly(dimethyl siloxane) membrane. *Desalination*, *233*: 286–294.
16. Flory, P.J. (1953) *Principles of Polymer Chemistry*; Cornell University Press: Ithaca; New York, 511–514.

17. Lue, S.J.; Wang, S.F.; Wang, L.D.; Chen, W.W.; Du, K.M.; Wu, S.Y. (2008) Diffusion of multicomponent vapors in a poly(dimethyl siloxane) membrane. *Desalination*, *233*: 277–285.
18. Balik, C.M. (1996) On the extraction of diffusion coefficients from gravimetric data for sorption of small molecules by polymer thin films. *Macromolecules*, *29*: 3025–3029.
19. Crank, J. (1975) *The Mathematics of Diffusion;* 2nd Ed.; Clarendon Press: Oxford, U.K.
20. Lue, S.J.; Wang, F.J.; Hsiaw, S.Y. (2004) Pervaporation of benzene/cyclohexane mixtures using ion-exchange membrane containing copper ions. *J. Membrane Sci.*, *240*: 149–158.
21. Blume, I.; Schwering, P.J.F.; Mulder, M.H.V.; Smolders, C.A. (1991) Vapour sorption and permeation properties of poly (dimethylsiloxane) films. *J. Membrane Sci.*, *61*: 85–97.
22. Gref, R.; Nguyen, Q.T.; Néel, J. (1992) Influence of membrane properties on system performances in pervaporation under concentration polarization regime. *Sep. Sci. Technol.*, *27* (4): 467–491.
23. Alpers, A.; Keil, B.; Ludtke, O.; Ohlrogge, K. (1999) Organic vapor separation: process design with regards to high-flux membranes and the dependence on real gas behavior at high pressure applications. *Ind. Eng. Chem. Res.*, *38*: 3754–3760.
24. Wu, H.; Liu, L.; Pan, F.; Hu, C.; Jiang, Z. (2006) Pervaporative removal of benzene from aqueous solution through supramolecule calixarene filled PDMS composite membranes. *Sep. Purif. Technol.*, *51*: 352–358.
25. Greenlaw, F.W.; Prince, W.D.; Shelden, R.A.; Thompson, E.V. (1977) Dependence of diffusive permeation rates on upstream and downstream pressures I. Single component permeant. *J. Membrane Sci.*, *2*: 141–151.
26. Shelden, R.A.; Thompson, E.V. (1978) Dependence of diffusive permeation rates on upstream and downstream pressures III. Membrane selectivity and implications for separation processes. *J. Membrane Sci.*, *4*: 115–127.
27. Greenlaw, F.W.; Shelden, R.A.; Thompson, E.V. (1977) Dependence of diffusive permeation rates on upstream and downstream pressures: II. Two component permeate. *J. Membrane Sci.*, *2*: 333–348.
28. Van Krevelen, D.W.; Hoftyzer, P.J. (1976) *Properties of Polymers-Their Estimation and Correlation with Chemical Structure;* 2nd Ed.; Elsevier Scientific Publishing Co.: Amsterdam, Netherlands.
29. Lue, S.J.; Lee, D.T.; Chen, J.Y.; Hu, C.C.; Jean, Y.C.; Lai, J.Y. (2008) Diffusivity enhancement of water vapor in poly(vinyl alcohol)-fumed silica nano-composite membranes: Correlation with polymer crystallinity and free-volume properties. *J. Membrane Sci.*, *325*: 831–839.